Author Contributions:
Conceptualization: V. Turino, V. Magni, H. J. Kjøll, J. Jakob
Formal analysis: V. Turino
Investigation: V. Turino, V. Magni, H. J. Kjøll, J. Jakob
Methodology: V. Turino, V. Magni
Project Administration: V. Magni
Resources: V. Magni
Supervision: V. Magni
Validation: V. Magni, H. J. Kjøll, J. Jakob
Visualization: V. Turino, V. Magni, H. J. Kjøll, J. Jakob

The Effect of Magma Poor and Magma Rich Rifted Margins on Continental Collision Dynamics

V. Turino[1] , **V. Magni[2,3]**, **H. J. Kjøll[4]** , and **J. Jakob[5]**

[1]University of Miami, Rosenstiel School of Marine, Atmospheric, and Earth Science, Miami, FL, USA, [2]Department of Geosciences, The Centre for Earth Evolution and Dynamics (CEED), University of Oslo, Oslo, Norway, [3]Now at Norwegian Geotechnical Institute (NGI), Oslo, Norway, [4]Department of Geosciences, University of Oslo, Oslo, Norway, [5]Geological Survey of Norway (NGU), Trondheim, Norway

Abstract The transition between non-rifted continental lithosphere and oceanic lithosphere in rifted margins can display a wide range of characteristics, depending on the regional tectonic evolution. The velocity and duration of the rifting process as well as the geodynamic setting influence the properties and geometry of the margins, which are often grouped into two main categories: magma-poor and magma-rich. We show how different types of rifted margins can influence the dynamics of continental collision, focusing on the time and depth of slab break-off after collision and the fate of margin material. We find that rifted margins have a noticeable impact on subduction dynamics, as we observe large variability in slab break-off times and depths. In particular, the presence of a rifted margin can delay slab break-off to up to 60 Myr after the onset of collision. Our results show that a large portion of the weak crust of magma-poor margins is likely to detach from the subducting plate and accrete to the upper plate, while the dense and strong mafic and ultramafic component of magma-rich margins causes most of the margin to subduct and be lost into the mantle, leaving only a small fraction of transitional and oceanic crust at the surface. Therefore, the volume of accreted material is much larger when the margin is magma-poor than magma-rich, which is consistent with geological observations that fossil magma-poor rifted margins are preserved in many mountain ranges, whereas remnants of magma-rich rifted margins are scarce.

Plain Language Summary The transition between continental and oceanic lithosphere at rifted margins in nature is not a sharp boundary, but it is gradual and often characterized by the presence of altered crust. Such margins can be either magma-poor or magma-rich, depending on the volume and timing of magmatism during extension; in nature, we can find traces of rifted margins in collisional mountain belts, with magma-poor margins being more easily preserved than magma-rich ones. The available models for continental collision, however, do not often consider the presence of such margins. We model continental collision with the presence of a magma-poor or magma-rich rifted margin, aiming to provide an explanation for these observations and to see how the margins can affect the subduction process. We find that the presence of a rifted margin can have a significant impact on the evolution of the subduction system, with slab break-off being significantly delayed in all cases. In the models, we find that part of the margin is always transferred to the overriding plate, and our results show that magma-poor margins are more likely to be recovered, matching the observations that magma-poor margins are more easily preserved than magma-rich.

1. Introduction

The term continental collision refers to the closure of an ocean and subsequent mountain building (Turcotte & Schubert, 2014). This process results in the subduction of buoyant continental material, slowing down sinking of the slab in the upper mantle and eventually stopping the subduction process (Cloos, 1993; McKenzie, 1969). When continental lithosphere arrives at the trench, the continental crust may undergo deep burial; the amount of subducted continental material depends on the slab pull that the subducted oceanic part of the slab exerts (Regard et al., 2003). In contrast to older oceanic lithosphere, continental lithosphere is buoyant, and the continent will resist subduction, likely resulting in the break-off from the oceanic slab in response to tensile stress generated by the pull of the subducting oceanic lithosphere (e.g., Duretz et al., 2011; Huw Davies & von Blanckenburg, 1995; Magni et al., 2012; van Hunen & Allen, 2011). During continental collision, pieces of the subducting crust can detach from the slab and become part of the overriding plate in a process called accretion (Cloos, 1993), which can happen in several ways. In some cases, the crust is scraped off from the subducting plate during convergence

Writing – original draft: V. Turino, V. Magni, H. J. Kjøll, J. Jakob
Writing – review & editing: V. Turino, V. Magni, H. J. Kjøll, J. Jakob

and is transferred to the accretionary wedge at relatively shallow depths (e.g., Clift & Vannucchi, 2004; Vogt et al., 2013). Portions of the crust can also detach at larger depths, after undergoing subduction and can rise back through the subduction channel and/or being emplaced below the overriding plate, that is, underplating (e.g., Schliffke et al., 2019; Vogt et al., 2013) or relamination (Hacker et al., 2011).

The transition between oceanic and continental lithosphere in the subducting plate, marked by the presence of rifted margins, constitutes an important region in which deformation is accommodated during continental collision. Rifted margins are formed during rifting and can be extremely diverse. Depending on the volumes and/or timing of extension-related magmatism, two different end members of a spectrum of margins can be defined (Sapin et al., 2021): magma-poor (MP) and magma-rich (MR) (Franke, 2013; Menzies et al., 2002; Tugend et al., 2020). In particular, MP margins are formed when extension is accompanied by little magmatism, and they are often characterized by a long continent-ocean transition (COT) zone (>300 km; Whitmarsh et al., 2001), composed of highly stretched and thinned continental lithosphere (Figure 1a). On the other end, magma-rich margins contain large volumes of mafic extrusive and intrusive rocks emplaced in a short period of time leading up to the actual continental break-up (Callot et al., 2002; Kjøll, Andersen, et al., 2019). MR margins are also composed of a lower crustal body, identified as a high velocity zone (HVZ) with seismic p-waves $v_p > 7.3$ km/s (Franke, 2013) and usually interpreted as a lower crust highly intruded by mafic to ultra-mafic magma (Figure 1b) (e.g., Abdelmalak et al., 2017; Geoffroy, 2005; White & McKenzie, 1989). The oceanic crust outboard of the MR margins is generally thicker than normal, between 12 and 30 km, due to the excess magma production (Geoffroy, 2005; Tugend et al., 2020). Examples of a MR margin are the mid-Norwegian-central East Greenland conjugate margin (Geoffroy, 2005) and the Walvis margin (Namibia) with its conjugate SE-Brazil/Uruguay margin (Chauvet et al., 2021). Examples of magma-poor margins can be found in the Iberia-Newfoundland (Péron-Pinvidic & Manatschal, 2009) and the Angola-Esperito Santo conjugate margins (Peron-Pinvidic et al., 2013).

Once collision occurs, rifted margins are the first pieces of continent reaching the trench. Their architecture controls whether they subduct completely, partially accrete to the overriding plate and/or exhume after being subducted. Today, we observe fragments of rifted margins preserved in mountain belts. A fossil magma rich margin has been described from the Scandinavian Caledonides (Kjøll, Andersen, et al., 2019; Kjøll, Galland, et al., 2019) and geophysical data suggests the presence of a volcanic rifted margin in the Tasman Fold Belt System in eastern Australia (Direen & Crawford, 2003). Evidence of MP margins of the fossil Alpine Tethys margin are described from the Campo, Grosina and Bernina units in the Alps (Mohn et al., 2012) and in Alpine Corsica (Beltrando et al., 2013). This provides useful insights into the processes happening during continental subduction, accretion, and exhumation. For instance, we observe that MP rifted margins are more commonly preserved in mountain belts than MR margins (Manatschal, 2004).

Upon collision, different types of rifted margins will likely deform differently due to their diverse geometry, strength, and buoyancy. However, some models of continental collision completely ignore the presence of rifted margins by modeling an abrupt transition from continent to ocean (e.g., Magni et al., 2012; van Hunen & Allen, 2011). Other subduction models do incorporate a gradual transition from continent to ocean, but they do not discriminate between magma-poor and magma-rich margins nor discuss in details the effect that this transition has on subduction zone processes, such as topography, delamination and slab detachment (e.g., Balazs et al., 2022; Boonma et al., 2023; Duretz et al., 2011; Duretz et al., 2014; Duretz & Gerya, 2013; Erdős et al., 2022; Francois et al., 2014; Ueda et al., 2012). Importantly, the geometries and physical properties of rifted margins can be much more complex than a gradual transition (Kjøll, Galland, et al., 2019; Williams et al., 2019), and this complexity will be reflected in the subduction dynamics, suggesting the need to consider it in modeling studies.

To account for this, we employ dynamic subduction models to investigate the effect on subduction dynamics of different margin architectures, in particular its effect on slab break-off and on the accretion of margin material, and we highlight the differences that arise if the margin is magma-poor or magma-rich.

2. Methods

2.1. Governing Equations

We model subduction and continental collision in a two-dimensional Cartesian geometry. We describe the thermal and compositional convection in the mantle by solving the equations for the conservation of mass, energy, momentum and composition for an incompressible and viscous Boussinesq medium, using the finite element code Citcom (Moresi & Solomatov, 1995; Zhong et al., 2000).
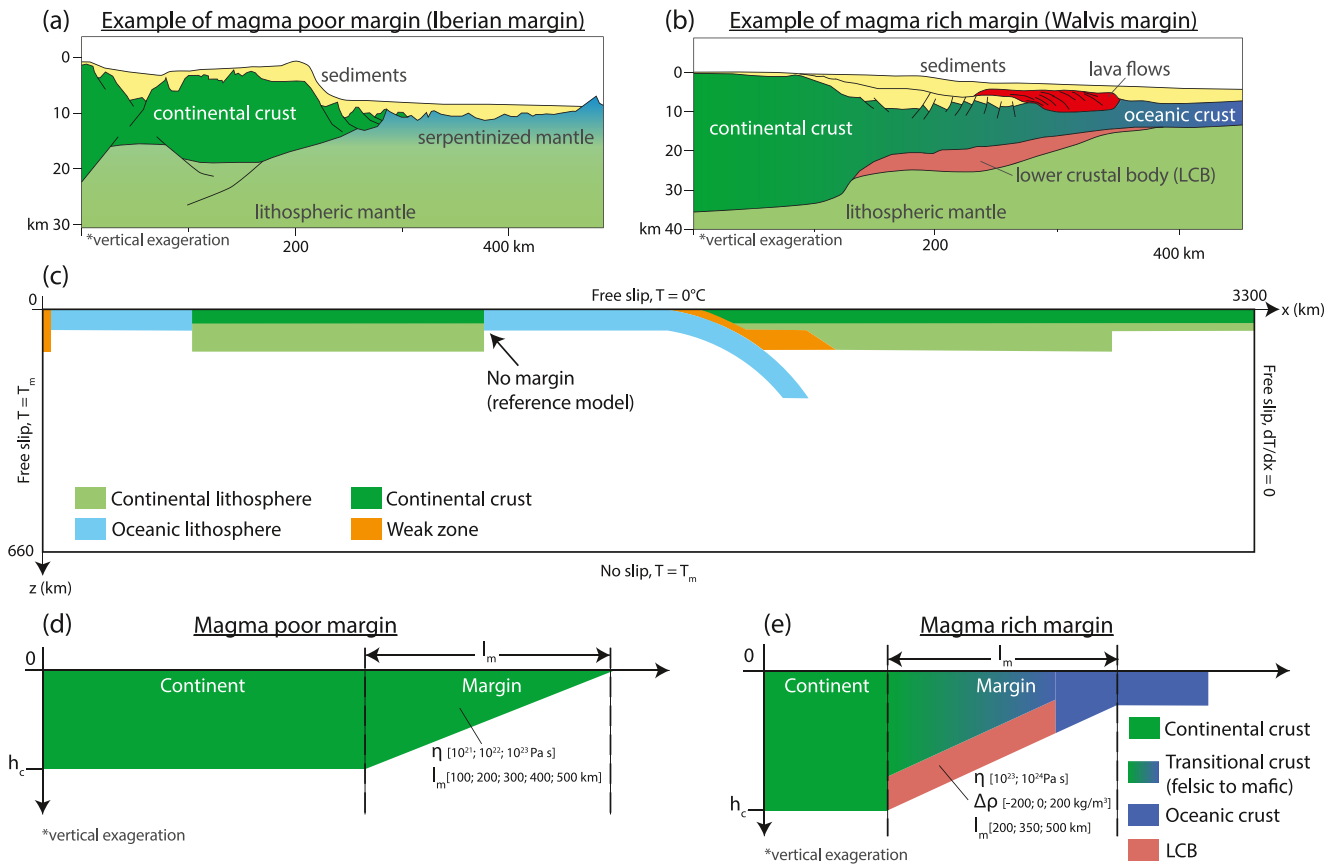
Figure 1. Schematic representation of (a) the Iberian magma-poor rifted margin and (b) the Walvis magma-rich rifted margin (Namibia; modified from Péron-Pinvidic & Manatschal, 2009; Blaich et al., 2011; Kjøll, 2019). (c) Initial setup of the reference model with boundary conditions and dimensions of the computational domain. The reference model has an abrupt continent-ocean transition (no modeled rifted margin). All other models include a rifted margin. (d) Crustal structure of modeled magma-poor margins and values of the explored parameters; viscosity (η) and margin length (l_m). (e) Crustal structure of the modeled magma-rich margins and values of the explored parameters; η and density contrast ($\Delta\rho$) of the lower crustal body (LCB) and l_m. The transitional crust is modeled with a gradual density change from continental to oceanic crustal density. For both magma-poor and magma-rich margins, the bottom of the lithosphere has the same shape as the Moho. h_c: crustal thickness.

$$\nabla \cdot u = 0$$

$$-\nabla p + \nabla \cdot \left[\eta \left(\nabla u + \nabla^T u \right) \right] + (RaT + RbC)e_z = 0$$

$$\frac{\partial T}{\partial t} + u \cdot \nabla T = \nabla^2 T$$

$$\frac{\partial C}{\partial t} + u \cdot \nabla C = 0$$

where u is the velocity, p is the deviatoric pressure, η is the viscosity, C is the composition, T is the temperature, and Ra and Rb are, respectively, the thermal and compositional Rayleigh number, defined as follows (see Table 1 for symbols):

$$Ra = \frac{\alpha \rho_0 g \Delta T h^3}{k \eta_0}$$

$$Rb = \frac{\delta \rho_c g h^3}{k \eta_0}$$

Table 1
List of Parameters With Values and Units and Description of the Mesh Used in the Models

Parameter	Symbol	Value	Unit
Velocity	u	–	(ms^{-1})
Deviatoric pressure	p	–	(Pa)
Viscosity	η	–	(Pa s)
Temperature	T	–	(°C)
Composition	C	0 or 1	–
Thermal Rayleigh number	Ra	4.4×10^6	–
Compositional Rayleigh number	Rb	1.7×10^7	–
Thermal expansion coefficient	α	3.5×10^{-5}	(K^{-1})
Reference density	ρ_0	3300	(kg m^{-3})
Density contrast	$\Delta\rho_c$	–	(kg m^{-3})
Gravitational acceleration	g	9.81	(m s^{-1})
Box height	h	660	(km)
Reference viscosity	η_0	10^{23}	(Pa s)
Thermal diffusivity	k	10^{-6}	(m^2 s^{-1})
Rheological pre-exponent	A_D	6.52×10^6	(Pa^{-n} s^{-1})
Strain rate	$\dot{\epsilon}$	–	(s^{-1})
Rheological power law exponent	n	1 (diff.c.), 3.5 (disl.c.)	–
Gas constant	R	8.3	(J K^{-1} mol^{-1})
Activation energy	E	360	(KJ mol^{-1})
Mesh resolution			
$\quad x < 40$, $x > 3260$ km		8	km
$\quad 1458 < x < 2224$ km		5	km
$\quad 40 < x < 1458$, $2224 < x < 3260$ km		~10	km
$\quad z < 450$ km ($z > 450$ km)		3 (6)	km

2.2. Model Setup

The starting point for this work is based on the model described in Magni et al. (2012), depicted in Figure 1c. The reference model describes a geometry with an abrupt transition between continent and ocean, thus, ignoring the presence of a rifted margin. We use this model for comparison to understand how results change when a more realistic margin is taken into account.

We model subduction in a 2D, 3,300 km × 660 km rectangular domain, corresponding to a box that extends from the Earth's surface (without taking the oceans into account) to the upper—lower mantle boundary. The lower mantle is not part of the domain. The mesh is not homogeneous and it is more refined where we need to resolve for high viscosity contrast or for small-scale features (see Table 1, the resolution goes from 10 × 10 km^2 elements to 3 × 3 km^2 elements). The overriding plate is entirely composed of continental lithosphere, with a 30 km thick continental crust. The subducting plate is described as an oceanic lithosphere and includes a continental block about 800 km long, initially located at a distance of 500 km from the position of the trench. The thickness of the continental crust in this block is 30 km in the models with magma-poor rifted margins and 40 km in all other models, because of the need to accurately resolve a more complex margin structure. The continental crust in both the subducting and overriding plate has a density contrast with respect to the mantle of $\Delta\rho = 500$ kg/m^3. Different materials in the models are tracked through passive tracers (Ballmer et al., 2007; Di Giuseppe et al., 2008). In particular, we use passive tracers to track the composition of continental crust and, when present, oceanic crust, transitional crust, and lower crustal body material. At the trench, the lithosphere reaches a depth of 260 km with a curvature radius of 500 km as this provides enough slab pull to initiate subduction, without the need to impose external forces to push the plates.

The initial thermal structure of the oceanic lithosphere is computed from the half-space cooling model for a 50 Ma plate (Turcotte & Schubert, 2014). For the continental lithosphere, the temperature increases linearly from 0°C at the surface to the mantle potential temperature $T_m = 1,350$°C at a depth of 150 km. The boundary conditions for the temperature require to have 0°C at the surface, dT/dx = 0 at the right boundary, and $T_m = 1,350$°C at the lower and left boundary. Radiogenic heat production in the crust is not taken into account, as we do not expect it to have a big effect on the model dynamic. The boundary conditions for the velocity are imposed to be free-slip everywhere but at the lower boundary, where there is a no-slip boundary condition. The assumption taken here is that because of its high viscosity, the lower mantle acts as a rigid boundary. A representation of the viscosity field and thermal structure for the reference model can be found in Figure S1 in Supporting Information S1.

2.3. Modeling Rifted Continental Margins

We model magma-poor and magma-rich margins by adding to the reference model a transitional area that gradually thins between the continent and the ocean. We parametrically vary the geometry and rheology of this region to describe the specific margin type considered (Figures 1d and 1e).

Magma poor (MP) margins are usually characterized by highly stretched, thinned, and faulted continental crust and are, thus, potentially weaker than the rest of the subducting plate. Moreover, their length across strike is variable and can reach values of >500 km; the Newfoundland margin, for example, is 420 km long (Peron-Pinvidic et al., 2013). Therefore, in our parametric study we vary the viscosity, assigning a fixed value, and the length of the MP rifted margin to understand what effects these two parameters have on the dynamics of continental collision. The viscosity of the continental crust at the rifted margin varies between 10^{21} and 10^{23} Pa s and the margin length varies from 100 to 500 km. For simplicity, from now on we will talk about the viscosity of the margins in relation to the reference viscosity $\eta_0 = 10^{23}$ Pa s. Therefore, we introduce the viscosity contrast $\eta_{m/0} = \eta_m / \eta_0$, where η_m is the viscosity of the continental crust at the rifted margin. In the MP models, then, the viscosity contrast assumes the values $\eta_{m/0} = 1, 10^{-1}, 10^{-2}$. We assume the transitional crust of MP margins to have the same density as continental crust, whereas its thickness linearly decreases from 30 km in the proximal margin (adjacent to the continental block) to 0 km where the margin ends and meets the oceanic lithosphere (Figure 1d).

In our models, magma-rich (MR) margins are modeled with a more complicate architecture than MP margins. A schematic representation of the models we implemented can be seen in Figure 1e. When modeling MR margins we have to take three features into account. Firstly, we model a transitional crust composed of a variable amount of mafic material (linearly, from 10% next to the continental crust, to 90% next to the oceanic crust). This variability is reflected in the models through density: we change the density linearly from the value assigned to continental crust to the value assigned to oceanic crust. Secondly, we describe a lower crustal body with a variable density contrast (-200 kg/m³; 0 kg/m³; 200 kg/m³) and viscosity (10^{23} Pa s; 10^{24} Pa s), corresponding to a high velocity zone for the seismic waves. Lastly, in MR models, an oceanic crust ($\Delta\rho = 300$ kg/m³) with thickness decreasing linearly from 20 to 7 km is considered to be part of the margin. The oceanic crust and the transitional crust both experience a basalt to eclogite transition at a depth of 40 km. Therefore, the density of the oceanic crust assumes the same density value of the mantle once this depth is reached, and the same happens to the transitional crust, in a percentage equal to the amount of mafic material it contains.

In the reference model and all models with MP margin, the oceanic crust is not present and the only type of crust considered is the continental one. In all the implemented models, the bottom of the lithospheric mantle of the rifted margin follows the same geometry as the crustal part.

2.4. Rheology

Rheology plays a crucial role in subduction dynamics and differences in rheological properties control the processes that we consider in this work, such as continental subduction, exhumation, and slab break-off.

The rheology of the mantle, which is both temperature and stress dependent, is described using diffusion and dislocation creep power laws (Hirth & Kohlstedt, 2003; Karato & Wu, 1993; Korenaga & Karato, 2008). For these two mechanisms, the viscosity can be written as:

$$\eta = A_D \dot{\epsilon}^{(1-n)/n} e^{-\frac{E}{RT}}$$

where A_D is the rheological pre-exponent (6.52×10^6 Pa^{-n} s^{-1}), $\dot{\epsilon}$ is the strain rate, E is the activation energy, R the gas constant, T the temperature and n is the rheological power law exponent, considered to be equal to one in case of diffusion creep and 3.5 in case of dislocation creep (Table 1). The reference value for the viscosity in the mantle, which varies as described, is 10^{20} Pa s.

We consider the lithosphere to be ductile at depth, with a rheological behavior that can be described in the same way as the mantle, and brittle near the surface. The brittle behavior of the lithosphere can be described as

$$\eta = \frac{\tau_y}{2\dot{\epsilon}}$$

where $\tau_y = \{\tau_0 + \mu p_0, \tau_{max}\}$ is the yield stress, τ_{max} the maximum yield stress and $\tau_0 + \mu p_0$ is the Byerlee law (Byerlee, 1978). To avoid non-physically realistic strengths at the surface, where the temperature is $T = 0°C$, we impose a maximum value for the viscosity η_{max}. At each point of the finite element grid, the effective viscosity is the minimum value of all those computed above.

A narrow weak zone (20 km wide, 230 km deep, viscosity 10^{20} Pa s), corresponding to an area with low viscosity, is introduced at the top left corner (orange in Figure 1a) to facilitate the motion of the subducting plate and simulate the presence of a mid-ocean ridge throughout the entire subduction process. We impose a 20 km wide weak zone (50 km deep, viscosity 10^{20} Pa s) with the same curvature of the slab to allow for decoupling between the plates (Figure 1a). The shape of this low viscosity zone remains fixed during the whole process, but its position changes according to the position of the slab (Magni et al., 2012). Below 50 km, to account for slab dehydration at depth of about 50–150 km, we model a weak mantle wedge which is 200 km wide and 150 km deep, whose maximum viscosity is 10^{20} Pa s. The shape of this weak region is a function of the shape of the slab and is, thus, not fixed (Magni et al., 2012).

3. Results

First, we describe the results of the model with no rifted margin. This result is used as a comparison for the models that do include rifted margins, which are described next. A list of all models with their margin's characteristics and key results is included in Table S1 in Supporting Information S1.

3.1. Reference Model

The time evolution of the reference model, which has an abrupt transition between continental and oceanic lithosphere, is described in Figure 2. At first the oceanic lithosphere sinks into the upper mantle and the slab reaches the bottom of the computational domain that represents the upper-lower mantle discontinuity. Then, the slab starts to flatten on the bottom of the domain. Continental collision occurs about 6 Myr after the beginning of the model (Figure 2b). This causes subduction to slow down because the continent is buoyant compared to the surrounding mantle and it resists subduction. At depth, however, the oceanic part of the slab is still pulling down. These two opposite forces create high stresses within the slab causing weakening and necking. Finally, about 20 Myr after collision, the slab breaks off at a depth of about 230 km and the oceanic crust continues to sink (Figure 2c). The continental crust reaches depths of about 100 km during subduction and partly exhumes after slab break-off (Figure 2d).

In all other models presented in this work, the subduction dynamics follow the same steps as described here. However, the timing and depth of slab break-off and the amount of subducted and exhumed continental crust (or transitional crust) significantly varies.

3.2. Magma Poor Margins

As described in Section 2.3, we model MP margins by including a transitional region of continental lithosphere that gradually thins toward the ocean. The time evolution of a MP rifted margin model is shown in Figure 3. This model has a margin with length 500 km and viscosity contrast $\eta_{m/0} = 10^{-2}$. In this model, slab break-off occurs about 50 Myr after the rifted margins first enters the trench, which is much later compared to the reference model (Figure 2). We observe that the crust that composes the rifted margin detaches from the lithospheric mantle, which continues to subduct, leaving the crust at the surface (Figure 3c) through delamination. Therefore, only a very small fraction of the margin crust is lost into the mantle during subduction, whereas most of it is accreted to the overriding plate (Figure 3d). This accreted material is either never subducted or it is subducted and then
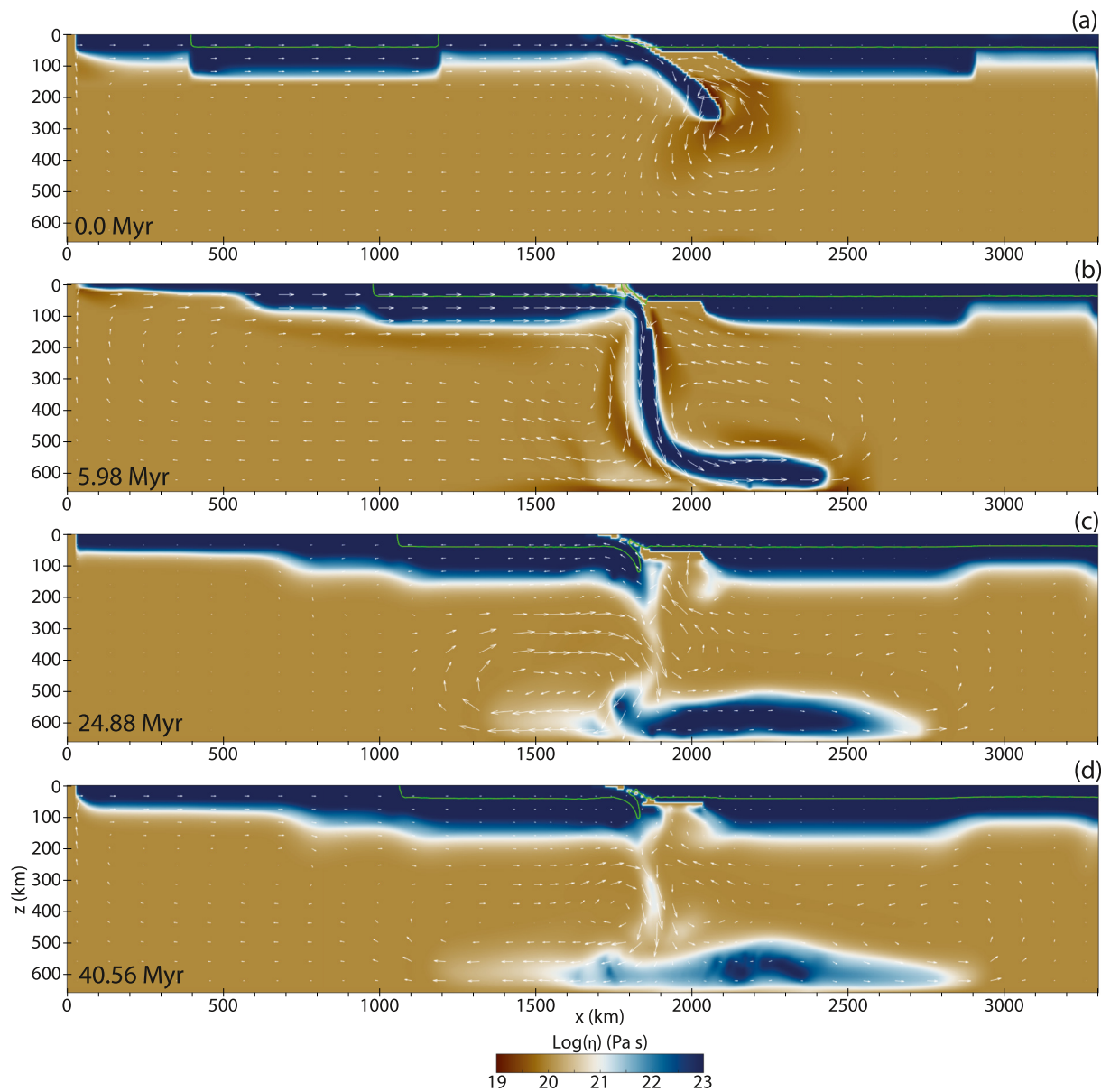
Figure 2. Time evolution of subduction and collision for the reference model that has an abrupt transition between continental and oceanic lithosphere. Colors represent the viscosity field. The green contour represents the continental crust, and the white arrows the velocity field. (a) is the initial setup, (b) shows the moment of continental collision, (c) corresponds to a time immediately after the slab break-off, and (d) represents the end of subduction.

exhumed or relaminated at later times. During collision of the margin, subduction slightly slows down, but does not cease because of the sinking of the lithospheric mantle part of the subducting plate while the positively buoyant crust stays at the surface, thus tensile stresses in the slab at depth remain low (Figure 3b). It is only when the margin ends and the continental block starts to subduct that the stresses in the slab increase enough for slab break-off to happen (Figure 3c). This type of dynamics is similar in all models with magma-poor margins, whether we change the length of the margin or its strength.

We perform a parametric study by changing the value of the margin length and viscosity, in order to understand what happens if the crust in the margin is as strong as the rest of the continental crust or if it is weaker, and what happens when the amount of margin material varies. Figures 4a–4d shows the final stage of subduction for models with MP margins with viscosity contrast $\eta_{m/0} = 10^{-2}$ and different margin lengths. One of the most noticeable features of this set of models is that accretion of the margin material to the overriding plate happens in all models (Figures 4a–4d). When the margin is short (100 km) we observe the accreted material only in a narrow
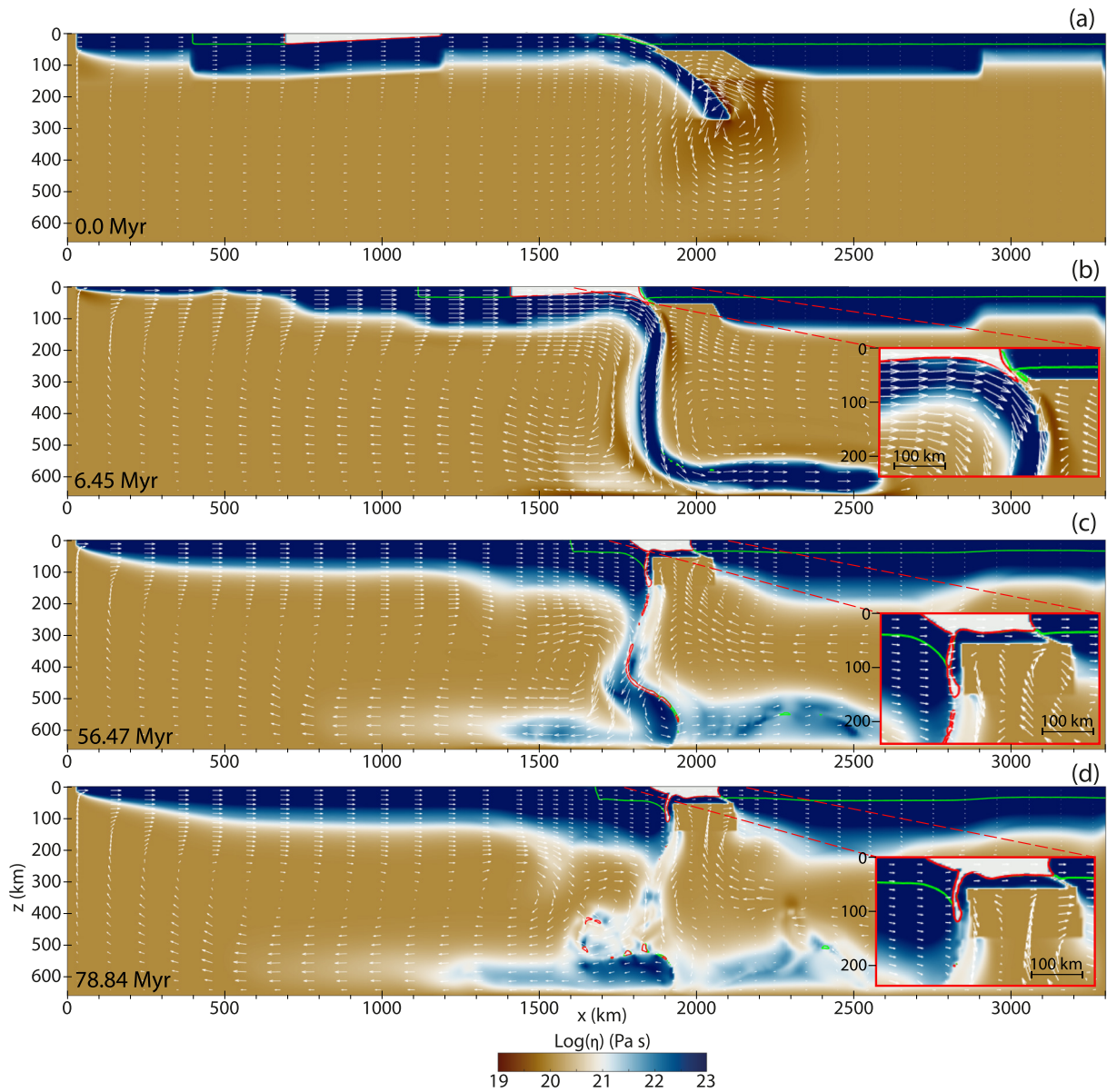
Figure 3. Time evolution of subduction and collision for magma-poor margins (model with margin length 500 km and $\eta_{m/0} = 10^{-2}$). Colors represent the viscosity field. The green contour represents the continental crust, the red contour the margin and the white arrows the velocity field. (a) is the initial setup, (b) shows the moment of continental collision, (c) corresponds to a time immediately after the slab break-off, and (d) represents the end of subduction.

region in the suture zone and in the subduction channel (Figure 4a). The longer the margin is, the more material is accreted to the overriding plate. For a 400 km long margin we observe a region of accreted margin material that extends 180 km from the suture zone (Figure 4d). In the model with the longest margin (500 km) the accreted crust extends to about 230 km from the trench (Figure 3d).

Decoupling of the margin crust from the lithospheric mantle happens in all models with a weak margin ($\eta_{m/0} = 10^{-2}$) resulting in very little margin material being lost into the mantle by subduction and most of it being accreted to the overriding plate (Figures 4a–4d, Figure S2a in Supporting Information S1). When the margin is slightly stronger ($\eta_{m/0} = 10^{-1}$), delamination is only partial because its viscosity leads to more coupling with the lithospheric mantle below it. Therefore, in this case, a larger part of the margin subducts, but it then exhumes after slab break-off (Figure S2b in Supporting Information S1). For both sets of models with $\eta_{m/0} = 10^{-2}$ and $\eta_{m/0} = 10^{-1}$ slab break-off happens only after the margin terminates and the continent arrives at the trench. This is not the case for models in which the margin has the same viscosity as the rest of the continent ($\eta_{m/0} = 1$). In
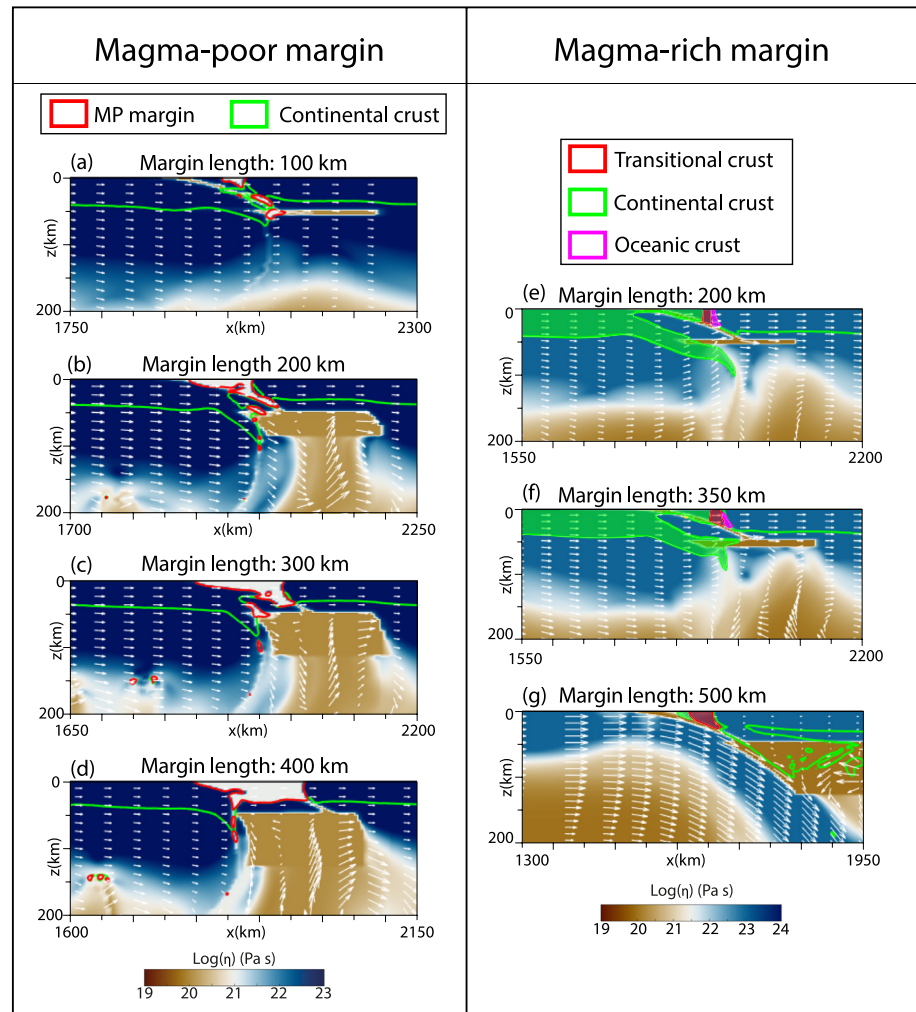
Figure 4. Accretion of margin material at the end of the model runs for models with (a) to (d): magma-poor margins with viscosity 10^{21} Pa s and margin length varying from 100 to 400 km and (e) to (g): magma-rich margins with $\Delta\rho = -200$ kg/m^3 and $\eta_{m/0} = 10$ Pa s and margin length varying from 200 to 500 km. These figures highlight the presence of accreted margin material on the overriding plate. Colors show the viscosity field, the contour colors are described in figure.

this case, except for when the margin is very short (100 km), subduction stops before the continent can reach the trench because the margin subducts together with the rest of the slab (i.e., no delamination) creating enough resistance to subduction to cause slab break-off (Figure S2c in Supporting Information S1). Therefore, the viscosity of the margin is also a factor in controlling the dynamics of continental subduction and accretion of margin material.

For the models with MP rifted margins, within the investigated parameter space, the time of slab break-off ranges between 10 and 60 Myr after collision and the depth of the break-off ranges between 250 and 450 km (Figures 5a and 5b). We notice that, for the same value of viscosity, break-off time increases with the length of the rifted margin (Figure 5b). For the slab break-off depth, however, it is more complicated to find a common trend. We observe that the depth value increases with margin length when the viscosity contrast of the margin is $\eta_{m/0} = 10^{-1}$, whereas it remains approximately constant, within a ~40 km range, for the weakest and strongest margins. Moreover, models with intermediate margin viscosity show a consistently higher slab break-off depth for the same margin length compared to the other viscosity values.

3.3. Magma Rich Margins

We modeled MR margins as characterized by the presence of a lower crustal body with variable density contrast (-200 kg/m^3; 0 kg/m^3; 200 kg/m^3) and viscosity (10^{23} Pa s; 10^{24} Pa s), underlying a transitional crust composed
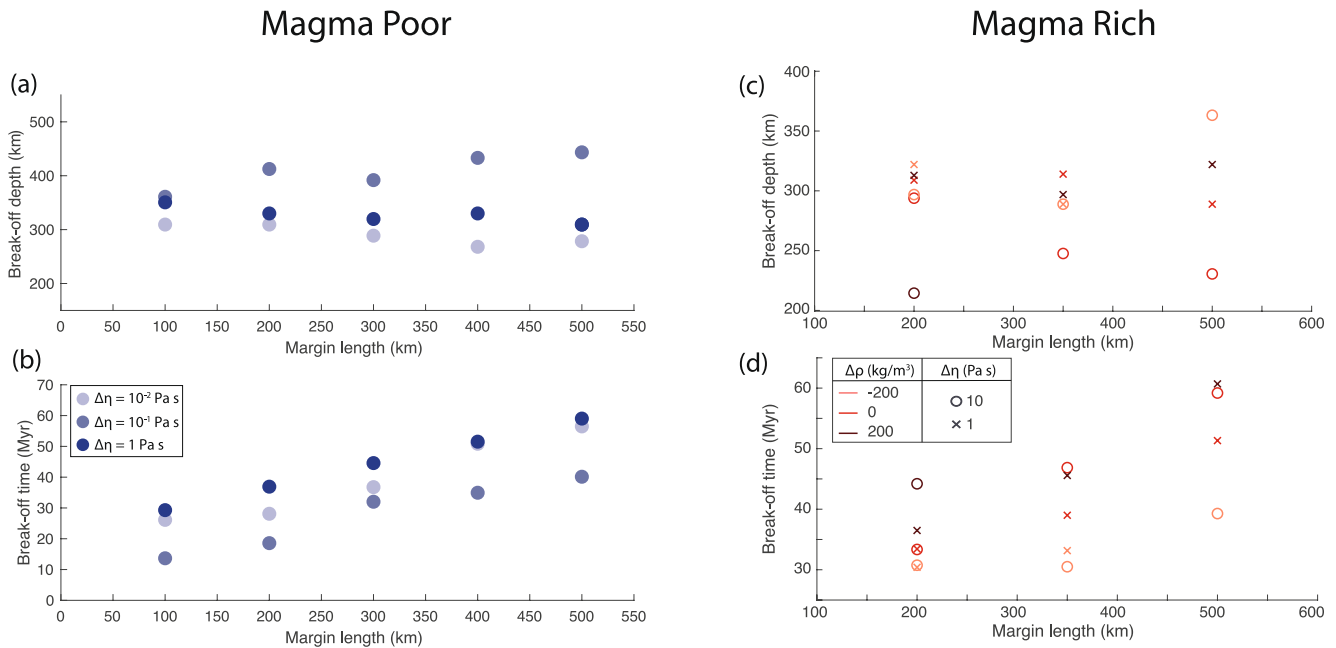
Figure 5. (a)–(b): Slab break-off (a) depth and (b) time as a function of the length of the margin for MP models with different viscosity of the margin crust. (c)–(d): Slab break-off (a) depth and (b) time as a function of the length of the margin for MR models. The color of the markers identifies the LCB density contrast and the shape of the marker its viscosity.

by a variable amount of mafic material. For this study, the length of the margin takes one of these values: 200 km, 350 km, 500 km. The model in Figure 6 corresponds to the median margin length of 350 km, LCB density contrasts of $\Delta\rho = -200$ kg/m³ and LCB viscosity $\eta = 10^{24}$ Pa s. The oceanic crust undergoes the basalt to eclogite transition at 40 km depth and subducts almost completely, although small remnants are preserved in the suture zone. When the margin reaches the trench, it easily subducts since the distal transitional crust is mostly mafic (Figure 1e), thus it provides only little resistance to subduction. However, due to the modeled increase in mafic material toward the ocean, the more margin material that is subducted, the more felsic the crust entering the trench is. As it starts subducting, a small portion of the transitional crust accretes to the overriding plate, whereas the rest undergoes eclogitization and subducts into the mantle (Figure 6c). The lower crustal body subducts completely and slab break-off occurs above it about 34 Myr after initial collision of the margin, which is again much later than in the reference model. Therefore, the lower crustal body is not preserved at all in the suture zone. After slab break-off, the continental crust that had subducted to depths of up to 300 km, rises back up as it is no longer pulled by the dense LCB and lithosphere, which results in underthrusting of continental crust below the suture zone (Figure 6d).

We conducted a parametric study of MR margins by varying the margin length, and the viscosity and density of the lower crustal body. As for the MP margin models, we observe accretion of the margin crust on the overriding plate (Figures 4e–4g), but with some fundamental differences compared to the MP case. In MR margins, in fact, the amount of accreted margin material is much lower than what we observe for the MP margin models. Indeed, even for the longest margin, the accreted transitional crust extends only a few tens of km (Figure 4g). This is because the presence of a strong and dense LCB and/or a partially mafic transitional crust increases slab pull and facilitates the subduction of most of the margin material. In this set of models, subduction slightly slows down when the rifted margin arrives at the trench, but does not cease, and the tensile stresses in the slab at depth remain low. Slab break-off usually occurs once the whole lower crustal body has been subducted. In models with a dense LCB ($\Delta\rho = -200$ kg/m³), slab break-off occurs just above the LCB, thus at the edge between the continent and its margin (Figure S3a in Supporting Information S1). In models with neutrally or positively buoyant LCB ($\Delta\rho = 0$ and 200 kg/m³), slab break-off usually occurs within the margin (Figures S3a and S3b in Supporting Information S1). However, the viscosity of the LCB plays a role too, with strong LCB favoring slab break-off above it. In a few models in which the LCB is strong ($\eta_{m/0} = 10$) slab break-off does not occur (Figure S4 in Supporting Information S1). This is due to computational limitations, since the viscosity of the LCB is, in
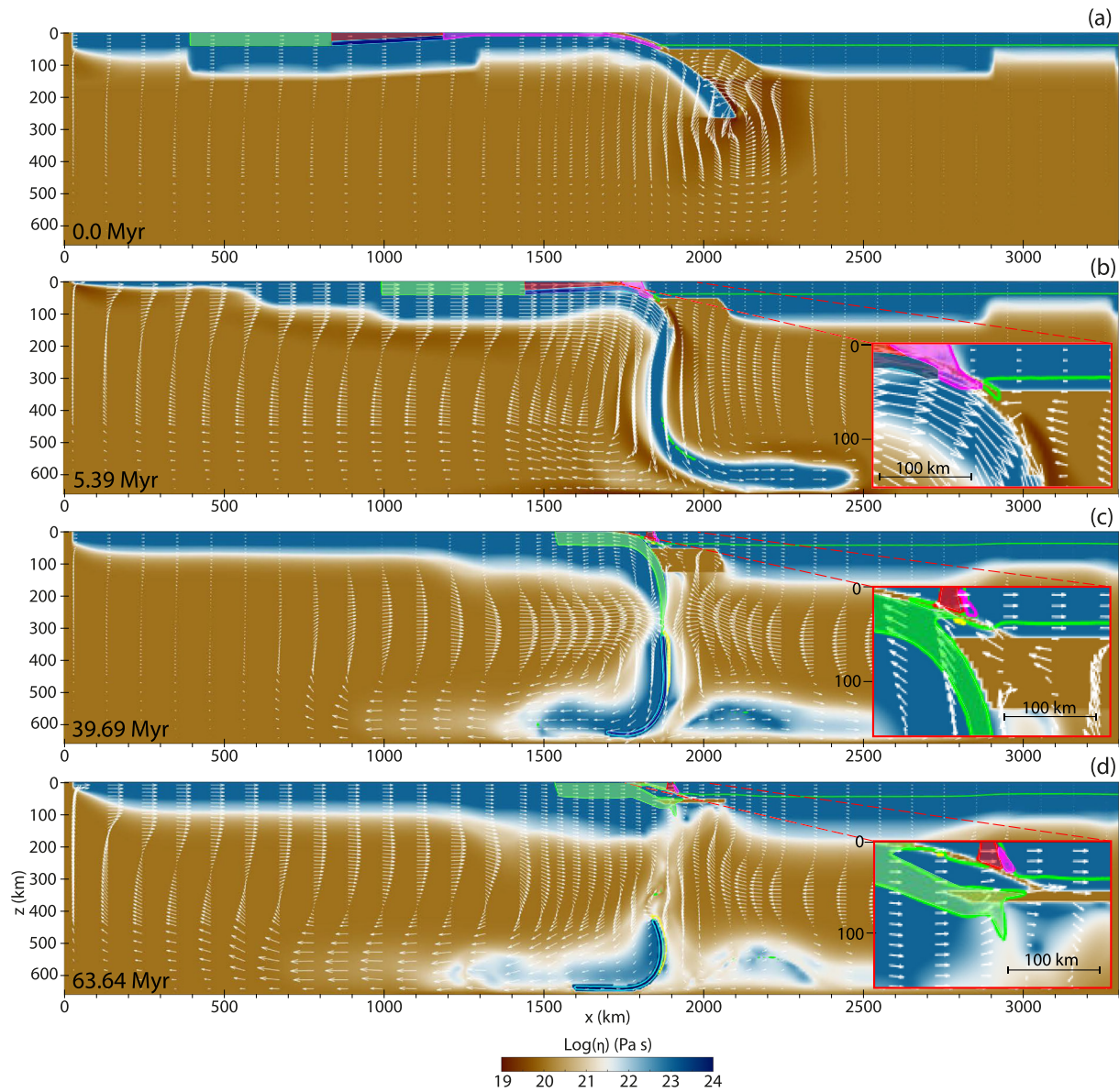
Figure 6. Time evolution of subduction and collision for magma-rich margins (model with margin length of 350 km, LCB density contrasts of $\Delta\rho = -200$ kg/m^3 and LCB viscosity $\eta = 10^{24}$ Pa s). Colors represent the viscosity field. The green contour represents the continental crust, the red contour the transitional crust before it transforms to eclogite, yellow contour is the transitional crust after eclogitization, the light blue contour the LCB, the magenta contour the oceanic crust, and the white arrows the velocity field. (a) is the initial setup, (b) shows the moment of continental collision, (c) corresponds to a time immediately after the slab break-off, and (d) represents the end of subduction.

fact, a constant value and it is not temperature- and stress-dependent, which prevents the LCB from breaking off, unlike the rest of the slab.

In the investigated parameter space, the range of slab break-off time for MR margin models spans from about 30 to 60 Myr, and the depth from about 200 to 360 km (Figures 5c and 5d). The time it takes for the slab to break-off increases when increasing the margin length. Furthermore, margins with a dense LCB are associated with shorter break-off times compared to those with neutrally and positively buoyant LCBs. This is because when the margin has subducted, it contributes to the slab pull forces, thus, a dense LCB results in high tensile stresses in the slab that favor break-off. The viscosity of the LCB controls where slab break-off occurs; within the margin when $\eta_{m/0} = 1$ (except when $\Delta\rho = -200$ kg/m^3) and above it when $\eta_{m/0} = 10$. Therefore, margins with a high viscosity body generally cause shallower break-offs as the slab tends to break above the margin.
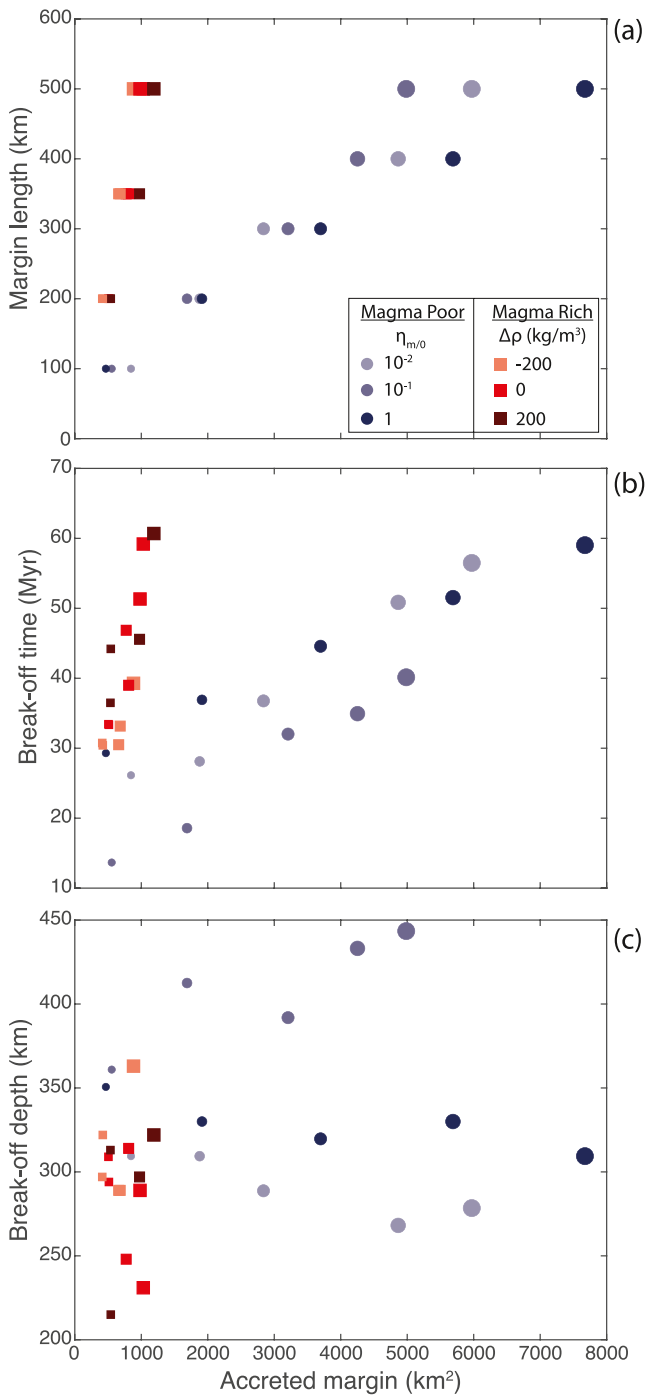
Figure 7. (a) Amount of accreted margin material as a function of the initial length of the margin for all models of this study (dots: magma-poor margins, square: magma-rich margins). (b) Time of slab break-off from the moment collision happens and (c) depth of slab break-off as a function of the amount of accreted margin material. Color of the markers represents the viscosity of the crust in MP margins and the density of lower crustal body in MR margins ($\Delta\rho = \rho_0 - \rho_{LCB}$). Size of the markers gradually increases with increasing of the initial length of the margin.

3.4. Accreted Margin Material

A key information we can extract from the models is how much of the initial margin material is preserved in the orogeny after collision ended. To quantitatively compare all the models, we define the amount of margin material preserved during the orogeny as the amount of margin crust that is found at a depth from 0 to 40 km at the end of the model run. This could either be margin material that has never been subducted to depths >40 km or material that did subduct but was subsequently exhumed.

We observe that the amount of preserved margin material is generally much higher in models with magma-poor margins than in those with magma-rich margins; for MP margins, it ranges from about 470 to 7,670 km^2, which corresponds to ~25%–75% of the initial margin material, whereas it stays below 1230 km^2 and 20% of the initial margin for all MR margins (Figure 7a, Table S1 in Supporting Information S1). All models, for both MP and MR margins, show increasingly higher volumes of preserved margin material with increasing of the initial length of the margin (Figure 7a). The volume of accreted MP margin material is consistently higher than that of MR margins, when keeping the initial length of the margin constant (Figure 7a).

The strength of the margin in MP margin models also has a crucial, albeit not straightforward, effect in controlling the amount of preserved margin material because it controls whether decoupling of the margin crust from the subducting lithospheric mantle occurs or not. One would expect models where delamination occurs to show a higher amount of preserved margin material, since the margin crust remains at the surface while the lithospheric mantle part of the margin subducts. Indeed, this is the case when comparing models with weak margins, in which delamination or partial delamination does occur; for the same margin length, more margin material is preserved for the weakest margins (i.e., $\eta_{m/0} = 10^{-2}$) compared to those with $\eta_{m/0} = 10^{-1}$. However, models with the strongest MP margins (i.e., $\eta_{m/0} = 1$), where delamination does not occur, show the largest amount of margin material preserved, except for the shortest margins. This might seem counterintuitive, but it is simply because slab break-off occurs before the continent reaches the trench, therefore part of the margin is preserved because it never even arrived at the suture zone. Therefore, in this case, the margin is not really accreted to the overriding plate, but it is preserved on the other side of the suture zone, within the subducting plate. For MR margins, models with lighter lower crustal bodies display a slightly higher amount of accreted material, though the difference with other MR models that have less dense LCB is very small (Figure 7a).

For both MP and MR margins, we observe a clear relationship between the amount of preserved margin material and the time of slab break-off; the more margin is preserved, the longer it takes for the slab to break off (Figure 7b). On the other hand, the depth of slab break-off does not seem to be related to the amount of preserved margin material (Figure 7c).

4. Discussion

Our results show that the architecture of a rifted margin strongly affects slab break-off and the likelihood of preserving portions of the margin in the geologic record. We find that, when the transition between continent and ocean is abrupt, slab break-off happens earlier and shallower compared to when a rifted margin is included in the models. Indeed, the presence of a rifted margin can delay slab break-off to up to 60 Myr after collision,

compared to the value of 10 Myr we obtain in the model with no margin (Table S1 in Supporting Information S1). We find that, keeping all other parameters fixed, the longer the margin is, the longer it takes for the slab to break-off (Figure 5). This is because in most models, except for those with strong MP margins, the sole subduction of the margin is not enough to cause slab break-off, which happens only after the continental block starts to subduct. Therefore, longer margins result in longer break-off times simply because it takes longer for the continent to reach the trench.

Of course, slab break-off time can also depend on many other factors, especially rheological parameters. However, several previous studies on slab break-off that focused on the rheological properties of the plates found slab break-off times of about 3–20 Myr after collision (e.g., Duretz et al., 2011; van Hunen & Allen, 2011), which are mostly smaller than the range we obtain in our models with rifted margins (10–60 Myr). These studies either did not include a rifted margin or did include one but kept its geometry and properties constant. This shows that taking into account the presence of rifted margins and their wide range of architectures into account in numerical models is important and that the time it takes for the slab to break off from the moment continental subduction starts can be much longer than previously suggested. The time between collision and slab break-off in natural cases ranges from fairly short times of 5–20 Myr for cases like the Alps, Apennines, and Carpathians, to higher values of 30–40 Myr for cases like the Himalayas and Scandinavian Caledonides (Garzanti et al., 2018; Jakob et al., 2022). The highest values of 50–60 Myr that we obtain in this study are perhaps less probable end-member scenarios and can be caused by the simplified rheology we use in our models (see 4.3). Similarly, the depth of slab break-off is also affected by the presence of a rifted margin, as it is about 230 km in our model with no margin, whereas it ranges from about 200 to 450 km in models with rifted margins. This depth range is within, but slightly deeper than the values of about 40–400 km found in previous studies (e.g., Duretz et al., 2011; van Hunen & Allen, 2011). The values of slab break-off time and depth obtained in this study have uncertainties and could vary if more parameters, such as those controlling the plate's rheology, the presence of sediments, or lateral heterogeneities along the trench in 3D were to be considered. However, we would still expect to obtain a wider range of values in models that include a rifted margin than those that do not.

4.1. Subduction of Magma-Poor Versus Magma-Rich Margins

The dynamics of collision are not solely affected by the presence of a rifted margin, but also the type of margin. We find that the ranges of slab break-off time and depth are wider when a continent with a magma-poor margin subducts (10–60 Myr and 250–450 km, respectively) than when the margin is magma-rich (30–60 Myr and 200–360 km) (Table S1 in Supporting Information S1). This reflects the wider variety of behaviors observed in models with magma-poor margins. Indeed, we find that models with weak magma-poor margins are prone to delamination of the margin crust, whereas those with strong crust do not show the same behavior. Delamination has an important effect on slab break-off because it changes the forces at play within the slab (e.g., Bird, 1978; Magni et al., 2013). By decoupling from the heavy lithospheric mantle and remaining at the surface, the margin crust, composed of buoyant continental crust, does not participate any longer in the slab pull force balance. Therefore, because the lightest part of the slab is not there, subduction continues until the margin terminates and the continent enters the trench, at which point the forces resisting subduction increase and slab break-off eventually occurs.

Although our models have a simplified rheology that assigns a fixed viscosity value to the margins, they show that the strength of the margin is crucial for the dynamics of continental subduction and that the weakness of the margin is the necessary ingredient to allow for relamination/delamination and margin preservation. Because of the extensional history of magma-poor rifted margins that results in a thinned and faulted continental crust, we argue that models with a weak crust best represent this type of margin. Therefore, we suggest that delamination, partial delamination or relamination of the margin crust are likely to be common processes when the continent that enters the subduction zone has a magma-poor type of margin.

Subduction of a magma-rich margin is very different because of its strong partly mafic crust and lower crustal body. In this case, not only the decoupling between margin crust and lithospheric mantle does not occur, but the dense mafic crust that transforms to eclogite and, in some models, the dense lower crustal body favor an almost complete subduction of the margin. Indeed, we find that very little margin material is preserved at the surface after collision has ended. Slab break-off occurs between the margin and the continent when the lower crustal body is dense and when it is strong, regardless of its buoyancy, whereas it occurs within the margin when it is neutrally

or positively buoyant and has the same viscosity as the rest of the lithosphere. Indeed, models with a strong LCB have a generally shallower break-off compared to models with $\eta_{m/0} = 1$. However, even if slab break-off happens above the margin, models with a dense LCB show a deeper slab break-off. This is because the negative buoyancy of the LCB plays a role as well by increasing slab pull forces, thus, enabling subduction of the continent to greater depths. This increase in slab pull forces causes a fast increase of tensile stresses in the slab, which, in turn, results in faster slab break-off when the LCB is dense. If the LCB is, instead, less dense than the mantle, its buoyancy acts against the slab pull, and break-off happens at later times.

Because of the uncertainties on the nature of the lower crustal body and its physical properties (Stab et al., 2016), it is difficult to estimate which of our models' parameters are more representative of magma-rich margins. As described in the introduction, the lower crustal body corresponds to a high-velocity zone (HVZ) for seismic waves and it is usually interpreted as lower continental crust highly intruded by mafic to ultra-mafic magma (Gernigon et al., 2004). Therefore, we assume this HVZ to be stronger or with the same viscosity as the rest of the plate. We tested different values of viscosity and density and the results did not change significantly. In fact, we find a common behavior among all models; when the margin is magma-rich, most of it subducts and is lost into the mantle, leaving only a small portion (<20%) preserved in the overriding plate. However, if this body or the whole margin is serpertinized and/or highly faulted, then the rheology can change and the margin could be overall weaker. Further work is required to better understand the properties of magma-rich margins and their effect on the dynamics of subduction.

4.2. Margin Preservation and Comparison With Natural Examples

The preservation potential of the margin at the end of collision is dependent on whether the subducted margin is magma-poor or magma-rich. We find that, regardless of the margin length, the volume of margin material preserved at the surface is always significantly larger for magma-poor margins (Figure 7). This is due to scraping-off of margin material at the trench during subduction, allowing part of the margin material to remain at the surface and resulting in a large region of accreted margin material in the upper plate that can extend up to 230 km from the suture. Instead, magma-rich margins almost completely subduct, leaving only small fragments of transitional and oceanic crust accreted to the upper plate, extending only a few tens of km from the suture. This is because MR margins are overall stronger and denser than MP margins, due to the presence of mafic and ultramafic material, which impedes crustal delamination and accretion to the upper plate. For both types of margin, parts of the preserved crust can be made of previously subducted crust that has exhumed after slab break-off and thus likely have experienced some degree of metamorphism.

The length of the margin has an important effect on the amount of preserved margin material, in that the longer the margin is, the larger volume is preserved. This is not surprising since long margins have more margin material to start with. However, for MP margins, it is not only the absolute value of preserved margin that increases with length, but also its percentage, reaching a fairly stable value of ∼50–60% with margins longer than 400 km (Figure S5 in Supporting Information S1). Longer margins also enhance decoupling between the plates and delay slab break-off. This explains the positive trend between the amount of accreted margin and slab break-off time. Importantly, even when a margin is long, if it is magma-rich, most of it is not preserved. This means that even though the length of the margin does have a control on its preservation, the most important controlling factor is its architecture and composition.

Accretion of margin material observed in our models is consistent with field observations (Manatschal, 2004; Manatschal & Müntener, 2009; Mohn et al., 2014) and modeling studies (Gómez-Romeu et al., 2023) that show that magma-poor margin material can be found in mountain ranges such as the Alps. In the Scandinavian Caledonides, the presence of both magma-rich and magma-poor margin material in different units along the orogeny has been suggested (e.g., Andersen et al., 2012; Jakob et al., 2019; Kjøll, Andersen, et al., 2019). These units are interpreted to include remnants of the rifted margin of Baltica formed during the formation of the Iapetus Ocean (e.g., Svenningsen, 2001; Tegner et al., 2019; Kjøll, 2020; R. A. Kumpulainen et al., 2021) that, eventually, were tectonized during the formation of the Scandian orogeny in the Silurian-Devonian. Estimates of the length of the rifted margin before collision span between 600 and 1,000 km (or more), although they are subject to high uncertainties (Gee, 1978; R. Kumpulainen et al., 1985; Jakob et al., 2022). Subduction of the margin likely started at ∼450 Ma, as suggested by the age of metamorphism of units interpreted to have originated at Baltica and subduction-related magmatism apparently ceased at ∼430 Ma (e.g.,

Andersen, 1998; Corfu et al., 2006; Klonowska et al., 2017; Root & Corfu, 2012). Finally, after the thinned continental crust of the rifted margin was consumed by subduction and/or accretion, the non-thinned part of the Baltica craton was pulled down to mantle depth by the Iapetus oceanic slab, which was followed by slab break-off at $\sim$410 $\pm$ 5 Ma (e.g., Hacker et al., 2010; Hacker & Gans, 2005). Therefore, the time between the first arrival of the margin at the trench and slab break-off is $\sim$40 Myr. This is in good agreement with our results that show that time of slab break-off can be considerably larger than previously thought when a rifted margin is accounted for.

Subduction of the Baltica margin follows a similar dynamic to that of most of our models, in that subduction continues until all the margin is consumed (either by subduction or accretion) and slab break-off only happens after the thick continent enters the trench. Through the process of delamination, the rifted margin that was originally part of the subducting plate, becomes part of the upper plate (Figures 3c and 3d). As the lithospheric mantle below continues to sink into the mantle and retreat, the corner flow brings asthenospheric mantle below the accreted margin. Numerical models of delamination showed that this could generate the conditions for mantle melting to occur and/or a temperature increase at the bottom of the upper plate (e.g., Faccenda et al., 2009; Göğüş & Ueda, 2018). This would explain the occurrence of magmatism until $\sim$430 Ma in the Caledonides after the onset of collision ($\sim$450 Ma) and the fact that some of these magmatic units intrude nappes that originally belonged to the subducting plate (Jakob et al., 2022).

It is important to note that the architecture of the Baltica margin was likely more complex than the two simplified endmembers of our study, as the tectonic units of the Scandinavian Caledonides include rock reminiscent of a magma-rich margin as well as highly stretched thin continental crust and exhumed mantle portions. Despite this simplification, our models are in good agreement with geological observations, demonstrating that the architecture of rifted margins play an important role in the dynamics of continental collision.

4.3. Model Limitations

The structure we assume for both MP and MR margins is meant to reproduce first-order features of the margin architecture, without taking into consideration some of the complications that characterize natural cases. In particular, a more complex rheology that includes mechanisms such as grain-size evolution, Peierls-creep, different flow laws for upper and lower crust and mantle serpentinization could further weaken the slab and affect the break-off process. For instance, we except that incorporating weakening mechanisms would accelerate slab break-off, lowering the upper limit of the time range we obtain. Nevertheless, we show that even with a simplified rheology our models manage to capture key differences in the behavior of collision of magma poor versus magma rich margins and to fit observations on preserved fossil margins.

5. Conclusions

We investigated how different types of rifted margins can influence the evolution of continental collision and to what extent they can be preserved in the upper plate. We found that the presence of rifted margins in numerical models of continental collision can significantly delay slab break-off and, to a less extent, deepen it compared to models that do not consider rifted margins. We observed a general trend indicating that by increasing the length of the margin, the time for the slab to break off increases as well. Moreover, we showed that the architecture of the margin has a significant impact on the tectonic processes that occur during the final stages of ocean closure and continental collision. More specifically, our models showed that, because of their weak crust, magma-poor rifted margins are prone to delaminate from the down-going plate, which allows for large portions of the margin to accrete to the overriding plate. The presence of strong and dense mafic and ultramafic material in magma-rich margins favors an almost complete subduction of the margin, with only small pieces of the transitional and oceanic crust being scraped off from the subducting plate and accreted to the upper plate. Therefore, magma-poor margins are more likely to be preserved than magma-rich ones after continental collision. Indeed, our study showed that models with magma-poor margins consistently have a much larger volume of preserved material compared to models with magma-rich margins of the same length. This is consistent with observations that indicate that remnants of fossil magma-poor margins are preserved in many mountain ranges, whereas it is rarer to find remnants of magma-rich margins.

Data Availability Statement

The modified version of the software CitCom (Moresi & Solomatov, 1995; Zhong et al., 2000) and the input files used for the models in this paper are available open access at the following Zenodo repository (Turino et al., 2023): https://doi.org/10.5281/zenodo.7931124.

References

Abdelmalak, M. M., Faleide, J. I., Planke, S., Gernigon, L., Zastrozhnov, D., Shephard, G. E., & Myklebust, R. (2017). The T-reflection and the deep crustal structure of the vøring margin, offshore mid-Norway. *Tectonics*, *36*(11), 2497–2523. https://doi.org/10.1002/2017TC004617

Andersen, T. B. (1998). Extensional tectonics in the Caledonides of southern Norway, an overview. *Tectonophysics*, *285*(3–4), 333–351. https://doi.org/10.1016/S0040-1951(97)00277-1

Andersen, T. B., Corfu, F., Labrousse, L., & Osmundsen, P. T. (2012). Evidence for hyperextension along the pre-Caledonian margin of Baltica. *Journal of the Geological Society*, *169*(5), 601–612. https://doi.org/10.1144/0016-76492012-011

Balázs, A., Faccenna, C., Gerya, T., Ueda, K., & Funiciello, F. (2022). The dynamics of Forearc – Back-arc basin subsidence: Numerical models and observations from Mediterranean subduction zones. *Tectonics*, *41*(5), e2021TC007078. https://doi.org/10.1029/2021TC007078

Ballmer, M. D., Van Hunen, J., Ito, G., Tackley, P. J., & Bianco, T. A. (2007). Non-hotspot volcano chains originating from small-scale sublithospheric convection. *Geophysical Research Letters*, *34*(23). https://doi.org/10.1029/2007GL031636

Beltrando, M., Zibra, I., Montanini, A., & Tribuzio, R. (2013). Crustal thinning and exhumation along a fossil magma-poor distal margin preserved in Corsica: A hot rift to drift transition? *Lithos*, *168–169*, 99–112. https://doi.org/10.1016/J.LITHOS.2013.01.017

Bird, P. (1978). Initiation of intracontinental subduction in the Himalaya. *Journal of Geophysical Research*, *83*(B10), 4975–4987. https://doi.org/10.1029/JB083IB10P04975

Blaich, O. A., Faleide, J. I., & Tsikalas, F. (2011). Crustal breakup and continent-ocean transition at South Atlantic conjugate margins. *Journal of Geophysical Research*, *116*(B1), B01402. https://doi.org/10.1029/2010JB007686

Boonma, K., García-Castellanos, D., Jiménez-Munt, I., & Gerya, T. (2023). Thermomechanical modelling of lithospheric slab Tearing and its topographic response. *Frontiers in Earth Science*, *11*. https://doi.org/10.3389/feart.2023.1095229

Byerlee, J. (1978). Friction of rocks. *Rock Friction and Earthquake Prediction*, 615–626. https://doi.org/10.1007/978-3-0348-7182-2_4

Callot, J.-P., Geoffroy, L., & Brun, J.-P. (2002). Development of volcanic passive margins: Three-dimensional laboratory models. *Tectonics*, *21*(6), 21–213. https://doi.org/10.1029/2001TC901019

Chauvet, F., Sapin, F., Geoffroy, L., Ringenbach, J. C., & Ferry, J. N. (2021). Conjugate volcanic passive margins in the austral segment of the South Atlantic – Architecture and development. *Earth-Science Reviews*, *212*, 103461. https://doi.org/10.1016/J.EARSCIREV.2020.103461

Clift, P., & Vannucchi, P. (2004). Controls on tectonic accretion versus erosion in subduction zones: Implications for the origin and recycling of the continental crust. *Reviews of Geophysics*, *42*(2). https://doi.org/10.1029/2003rg000127

Cloos, M. (1993). *Lithospheric buoyancy and collisional orogenesis: Subduction of oceanic plateaus, continental margins, island arcs, spreading ridges, and seamounts*. Geological Society of America Bulletin. Retrieved from https://pubs.geoscienceworld.org/gsa/gsabulletin/article/105/6/715/182815/Lithospheric-buoyancy-and-collisional-orogenesis

Corfu, F., Torsvik, T. H., Andersen, T. B., Ashwal, L. D., Ramsay, D. M., & Roberts, R. J. (2006). Early Silurian mafic–ultramafic and granitic plutonism in contemporaneous flysch, Magerøy, northern Norway: U–Pb ages and regional significance. *Journal of the Geological Society*, *163*(2), 291–301. https://doi.org/10.1144/0016-764905-014

Di Giuseppe, E., Van Hunen, J., Funiciello, F., Faccenna, C., & Giardini, D. (2008). Slab stiffness control of trench motion: Insights from numerical models. *Geochemistry, Geophysics, Geosystems*, *9*(2). https://doi.org/10.1029/2007GC001776

Direen, N. G., & Crawford, A. J. (2003). Fossil seaward-dipping reflector sequences preserved in southeastern Australia: A 600 Ma volcanic passive margin in eastern Gondwanaland. *Journal of the Geological Society*, *160*(6), 985–990. https://doi.org/10.1144/0016-764903-010

Duretz, T., Gerya, T. V., & May, D. A. (2011). Numerical modelling of spontaneous slab breakoff and subsequent topographic response. *Tectonophysics*, *502*(1–2), 244–256. https://doi.org/10.1016/J.TECTO.2010.05.024

Duretz, T., & Gerya, T. V. (2013). Slab detachment during continental collision: Influence of crustal rheology and interaction with lithospheric delamination. *Tectonophysics, TOPO-EUROPE III*, *602*, 124–140. https://doi.org/10.1016/j.tecto.2012.12.024

Duretz, T., Gerya, T. V., & Spakman, W. (2014). Slab detachment in laterally varying subduction zones: 3-D numerical modeling. *Geophysical Research Letters*, *41*(6), 1951–1956. https://doi.org/10.1002/2014GL059472

Erdős, Z., Zoltán, R. S., & Ritske, S. (2022). Huismans, and Claudio Faccenna. Wide versus narrow back-arc rifting: Control of subduction velocity and convective back-arc thinning. *Tectonics*, *41*(6), e2021TC007086. https://doi.org/10.1029/2021TC007086

Faccenda, M., Minelli, G., & Gerya, T. V. (2009). Coupled and decoupled regimes of continental collision: Numerical modeling. *Earth and Planetary Science Letters*, *278*(3–4), 337–349. https://doi.org/10.1016/j.epsl.2008.12.021

François, T., Burov, E., Agard, P., & Meyer, B. (2014). Buildup of a dynamically supported orogenic plateau: Numerical modeling of the Zagros/Central Iran case study. *Geochemistry, Geophysics, Geosystems*, *15*(6), 2632–2654. https://doi.org/10.1002/2013GC005223

Franke, D. (2013). Rifting, lithosphere breakup and volcanism: Comparison of magma-poor and volcanic rifted margins. *Marine and Petroleum Geology*, *43*, 63–87. https://doi.org/10.1016/J.MARPETGEO.2012.11.003

Garzanti, E., Radeff, G., & Malusà, M. G. (2018). Slab breakoff: A critical appraisal of a geological theory as applied in space and time. *Earth-Science Reviews*, *177*, 303–319. https://doi.org/10.1016/j.earscirev.2017.11.012

Gee, D. G. (1978). Nappe displacement in the Scandinavian Caledonides. *Tectonophysics*, *47*(3–4), 393–419. https://doi.org/10.1016/0040-1951(78)90040-9

Geoffroy, L. (2005). Volcanic passive margins. *Comptes Rendus Geoscience*, *337*(16), 1395–1408. https://doi.org/10.1016/j.crte.2005.10.006

Gernigon, L., Ringenbach, J.-C., Planke, S., & Le Gall, B. (2004). Deep structures and breakup along volcanic rifted margins: Insights from integrated studies along the outer Vøring basin (Norway). *Marine and Petroleum Geology*, *21*(3), 363–372. https://doi.org/10.1016/j.marpetgeo.2004.01.005

Göğüş, O. H., & Ueda, K. (2018). Peeling back the lithosphere: Controlling parameters, surface expressions and the future directions in delamination modeling. *Journal of Geodynamics*, *117*, 21–40. https://doi.org/10.1016/j.jog.2018.03.003

Gómez-Romeu, J., Jammes, S., Ducoux, M., Lescoutre, R., Calassou, S., & Masini, E. (2023). Inverted magma-rich versus magma-poor rifted margins: Implications for early orogenic systems 1. *tekt*. https://doi.org/10.55575/tektonika2023.1.1.12

Hacker, B. R., Andersen, T. B., Johnston, S., Kylander-Clark, A. R. C., Peterman, E. M., Walsh, E. O., & Young, D. (2010). High-temperature deformation during continental-margin subduction & exhumation: The ultrahigh-pressure Western Gneiss Region of Norway. *Tectonophysics*, *480*(1–4), 149–171. https://doi.org/10.1016/J.TECTO.2009.08.012

Hacker, B. R., & Gans, P. B. (2005). Continental collisions and the creation of ultrahigh-pressure terranes: Petrology and thermochronology of nappes in the central Scandinavian Caledonides. *GSA Bulletin*, *117*(1–2), 117–134. https://doi.org/10.1130/B25549.1

Hacker, B. R., Kelemen, P. B., & Behn, M. D. (2011). Differentiation of the continental crust by relamination. *Earth and Planetary Science Letters*, *307*(3), 501–516. https://doi.org/10.1016/j.epsl.2011.05.024

Hirth, G., & Kohlstedf, D. (2003). Rheology of the upper mantle and the mantle wedge: A view from the experimentalists. *Geophysical Monograph-American Geophysical Union*, *138*, 83–105. https://doi.org/10.1029/138gm06

Huw Davies, J., & Von Blanckenburg, F. (1995). Slab breakoff: A model of lithosphere detachment and its test in the magmatism and deformation of collisional orogens. *Earth and Planetary Science Letters*, *129*(1–4), 85–102. https://doi.org/10.1016/0012-821X(94)00237-S

Jakob, J., Andersen, T. B., & Kjøll, H. J. (2019). A review and reinterpretation of the architecture of the South and South-central Scandinavian Caledonides—A magma-poor to magma-rich transition and the significance of the reactivation of rift inherited structures. *Earth-Science Reviews*, *192*, 513–528. https://doi.org/10.1016/j.earscirev.2019.01.004

Jakob, J., Andersen, T. B., Mohn, G., Jørgen Kjøll, H., Beyssac, O., Orogeny, S., & Kuiper, S. (2022). Revised tectono-stratigraphic scheme for the Scandinavian Caledonides and its implications for our understanding of the Scandian orogenystratigraphic scheme for the Scandinavian Caledonides and its implications for our understanding of the. *Geological Society of America*. https://doi.org/10.1130/2022.2554(14)

Karato, S. I., & Wu, P. (1993). Rheology of the upper mantle: A synthesis. *Science*, *260*(5109), 771–778. https://doi.org/10.1126/science.260.5109.771

Kjøll, H. J. (2019). Neoproterozoic to lower Paleozoic evolution of the pre-Caledonian magma-rich margin of Baltica. Retrieved from https://www.duo.uio.no/handle/10852/70340?locale-attribute=en

Kjøll, H. J. (2020). Late Neoproterozoic basin evolution of the magma rich Iapetus margin of Baltica. *Norwegian Journal of Geology*. https://doi.org/10.17850/NJG100-1-6

Kjøll, H. J., Andersen, T. B., Corfu, F., Labrousse, L., Tegner, C., Abdelmalak, M. M., & Planke, S. (2019). Timing of breakup and thermal evolution of a pre-Caledonian Neoproterozoic exhumed magma-rich rifted margin. *Wiley Online Library*, *38*(6), 1843–1862. https://doi.org/10.1029/2018TC005375

Kjøll, H. J., Galland, O., Labrousse, L., & Andersen, T. B. (2019). Emplacement mechanisms of a dyke swarm across the brittle-ductile transition and the geodynamic implications for magma-rich margins. *Earth and Planetary Science Letters*, *518*, 223–235. https://doi.org/10.1016/J.EPSL.2019.04.016

Klonowska, I., Janák, M., Majka, J., Petrík, I., Froitzheim, N., Gee, D. G., & Sasinková, V. (2017). Microdiamond on Åreskutan confirms regional UHP metamorphism in the Seve nappe complex of the Scandinavian Caledonides. *Journal of Metamorphic Geology*, *35*(5), 541–564. https://doi.org/10.1111/JMG.12244

Korenaga, J., & Karato, S. I. (2008). A new analysis of experimental data on olivine rheology. *Journal of Geophysical Research*, *113*(B2). https://doi.org/10.1029/2007jb005100

Kumpulainen, R., Nystuen, J. P., Gee, D. G., & Sturt, B. A. (1985). Late Proterozoic basin evolution and sedimentation in the westernmost part of Baltoscandia. The Caledonide Orogen—Scandinavia and related areas. Retrieved from https://scholar.google.com/scholar?hl=en&as_sdt=0%2C10&q=kumpulainen+nystuen+1985&btnG=#d=gs_cit&t=1683910609505&u=%2Fscholar%3Fq%3Dinfo%3AeP6Dn2cgcrQ-J%3Ascholar.google.com%2F%26output%3Dcite%26scirp%3D0%26hl%3Den

Kumpulainen, R. A., Hamilton, M. A., Söderlund, U., & Nystuen, J. P. (2021). U-Pb baddeleyite age for the Ottfjället dyke swarm, central Scandinavian Caledonides: New constraints on Ediacaran opening of the Iapetus Ocean and glaciations on Baltica. *Gff*, *143*(1), 40–54. https://doi.org/10.1080/11035897.2021.1888314

Magni, V., Faccenna, C., Van Hunen, J., & Funiciello, F. (2013). Delamination vs. break-off: The fate of continental collision. *Geophysical Research Letters*, *40*(2), 285–289. https://doi.org/10.1002/GRL.50090

Magni, V., Van Hunen, J., Funiciello, F., & Faccenna, C. (2012). Numerical models of slab migration in continental collision zones. *Solid Earth*, *3*(2), 293–306. https://doi.org/10.5194/se-3-293-2012

Manatschal, G. (2004). New models for evolution of magma-poor rifted margins based on a review of data and concepts from West Iberia and the Alps. *International Journal of Earth Sciences*, *93*(3), 432–466. https://doi.org/10.1007/s00531-004-0394-7

Manatschal, G., & Müntener, O. (2009). A type sequence across an ancient magma-poor ocean-continent transition: The example of the western Alpine Tethys ophiolites. *Tectonophysics*, *473*(1–2), 4–19. https://doi.org/10.1016/j.tecto.2008.07.021

McKenzie, D. P. (1969). Speculations on the Consequences and causes of plate motions. *Geophysical Journal International*, *18*(1), 1–32. https://doi.org/10.1111/j.1365-246X.1969.tb00259.x

Menzies, M. A., Klemperer, S. L., Ebinger, C. J., & Baker, J. (2002). Characteristics of volcanic rifted margins. *Special Papers (Geological Society of America)*, *362*, 1–14. https://doi.org/10.1130/0-8137-2362-0.1

Mohn, G., Manatschal, G., Beltrando, M., & Haupert, I. (2014). The role of rift-inherited hyper-extension in Alpine-type orogens. *Wiley Online Library*, *26*(5), 347–353. https://doi.org/10.1111/ter.12104

Mohn, G., Manatschal, G., Beltrando, M., Masini, E., & Kusznir, N. (2012). Necking of continental crust in magma-poor rifted margins: Evidence from the fossil Alpine Tethys margins. *Tectonics*, *31*(1). https://doi.org/10.1029/2011TC002961

Moresi, L. N., & Solomatov, V. S. (1995). Numerical investigation of 2D convection with extremely large viscosity variations. *Physics of Fluids*, *7*(9), 2154–2162. https://doi.org/10.1063/1.868465

Péron-Pinvidic, G., & Manatschal, G. (2009). The final rifting evolution at deep magma-poor passive margins from Iberia-Newfoundland: A new point of view. *International Journal of Earth Sciences*, *98*(7), 1581–1597. https://doi.org/10.1007/s00531-008-0337-9

Peron-Pinvidic, G., Manatschal, G., & Osmundsen, P. T. (2013). Structural comparison of archetypal Atlantic rifted margins: A review of observations and concepts. *Marine and Petroleum Geology*, *43*, 21–47. https://doi.org/10.1016/j.marpetgeo.2013.02.002

Regard, V., Faccenna, C., Martinod, J., Bellier, O., & Thomas, J.-C. (2003). From subduction to collision: Control of deep processes on the evolution of convergent plate boundary. *Journal of Geophysical Research*, *108*(B4), 2208. https://doi.org/10.1029/2002JB001943

Root, D., & Corfu, F. (2012). U-Pb geochronology of two discrete Ordovician high-pressure metamorphic events in the Seve Nappe Complex, Scandinavian Caledonides. *Contributions to Mineralogy and Petrology*, *163*(5), 769–788. https://doi.org/10.1007/S00410-011-0698-0/FIGURES/11

Sapin, F., Ringenbach, J. C., & Clerc, C. (2021). Rifted margins classification and forcing parameters. *Scientific Reports*, *11*(1), 8199. https://doi.org/10.1038/s41598-021-87648-3

Schliffke, N., Van Hunen, J., Magni, V., & Allen, M. B. (2019). The role of crustal buoyancy in the generation and emplacement of magmatism during continental collision. *Geochemistry, Geophysics, Geosystems*, *20*(11), 4693–4709. https://doi.org/10.1029/2019GC008590

Stab, M., Bellahsen, N., Pik, R., Quidelleur, X., Ayalew, D., & Leroy, S. (2016). Modes of rifting in magma-rich settings: Tectono-magmatic evolution of Central Afar. *Tectonics*, *35*(1), 2–38. https://doi.org/10.1002/2015TC003893

Svenningsen, O. M. (2001). Onset of seafloor spreading in the Iapetus Ocean at 608 Ma: Precise age of the Sarek dyke swarm, northern Swedish Caledonides. *Precambrian Research*, *110*(1–4), 241–254. https://doi.org/10.1016/S0301-9268(01)00189-9

Tegner, C., Andersen, T. B., Kjøll, H. J., Brown, E. L., Hagen-Peter, G., Corfu, F., et al. (2019). A mantle plume origin for the Scandinavian dyke complex: A "piercing point" for 615 Ma plate reconstruction of Baltica? *Wiley Online Library*, *20*(2), 1075–1094. https://doi.org/10.1029/2018GC007941

Tugend, J., Gillard, M., Manatschal, G., Nirrengarten, M., Harkin, C., Epin, M. E., et al. (2020). Reappraisal of the magma-rich versus magma-poor rifted margin archetypes. *Geological Society Special Publication*, *476*(1), 23–47. https://doi.org/10.1144/SP476.9

Turcotte, D., & Schubert, G. (2014). Geodynamics. *Geodynamics*. https://doi.org/10.1017/CBO9780511843877

Turino, Valeria, Magni, V., Kjøll, H. J., & Jakob, J. (2023). Code and input files for "the effect of magma poor and magma rich rifted margins on continental collision dynamics". [Software]. Zenodo. https://doi.org/10.5281/zenodo.7931124

Ueda, K., Gerya, T. V., & Burg, J.-P. (2012). Delamination in collisional orogens: Thermomechanical modeling. *Journal of Geophysical Research*, *117*, B8. https://doi.org/10.1029/2012JB009144

Van Hunen, J., & Allen, M. B. (2011). Continental collision and slab break-off: A comparison of 3-D numerical models with observations. *Earth and Planetary Science Letters*, *302*(1–2), 27–37. https://doi.org/10.1016/J.EPSL.2010.11.035

Vogt, K., Castro, A., & Gerya, T. (2013). Numerical modeling of geochemical variations caused by crustal relamination. *Geochemistry, Geophysics, Geosystems*, *14*(2), 470–487. https://doi.org/10.1002/ggge.20072

White, R., & McKenzie, D. (1989). Magmatism at rift zones: The generation of volcanic continental margins and flood basalts. *Journal of Geophysical Research*, *94*(B6), 7685–7729. https://doi.org/10.1029/JB094IB06P07685

Whitmarsh, R. B., Manatschal, G., & Minshull, T. A. (2001). Evolution of magma-poor continental margins from rifting to seafloor spreading. *Nature*, *413*(6852), 150–154. https://doi.org/10.1038/35093085

Williams, S. E., Whittaker, J. M., Halpin, J. A., & Müller, R. D. (2019). Australian-Antarctic breakup and seafloor spreading: Balancing geological and geophysical constraints. *Earth-Science Reviews*, *188*, 41–58. https://doi.org/10.1016/J.EARSCIREV.2018.10.011

Zhong, S., Zuber, M. T., Moresi, L., & Gurnis, M. (2000). Role of temperature-dependent viscosity and surface plates in spherical shell models of mantle convection. *Journal of Geophysical Research*, *105*(B5), 11063–11082. https://doi.org/10.1029/2000JB900003